Deep Resources Engineering 3 (2026) 100204

Contents lists available at ScienceDirect

Deep Resources Engineering

journal homepage: www.keaipublishing.com/en/journals/deepre/

Full length article

An integrated intelligent long-term device for the borehole monitoring of deformation and evolution of fractures in rock masses

Jun Zhao [a,b,*], Jiang-Long Zhao [a,b], Xia-Ting Feng [a,b], Yue Guo [a,b], Xiao-Jun Zhang [a,b], Hong-Wei Xiang [a,b]

[a] State Key Laoratory of Intelligent Deep Metal Mining and Equipment, Northeastern University, Shenyang 110819, China
[b] Key Laboratory of Liaoning Province on Deep Engineering and Intelligent Technology, Northeastern University, Shenyang 110819, China

ARTICLE INFO

Keywords:
Deformation
Fracture
Borehole wall
Adaptive lifting structure
In-situ intelligent continuous monitoring

ABSTRACT

To solve the problems of complex operation, low efficiency, and lagging information collection in rock mass disaster monitoring, an integrated monitoring device is developed, which can simultaneously collect information related to the deformation and fracture of boreholes in rock mass. The device has broken through six key technologies: (1) an adaptive lifting structure is established to achieve stable movement in boreholes in rock mass under different apertures, inclination angles and complex environments; (2) a integrated monitoring probe is developed, which can synchronously monitor borehole deformation and fracture characteristics identification as well as capture co-evolution; (3) high-precision measurement technology was invented to solve the problem of inaccurate positioning of deep rock deformation and fractures; (4) overcoming the problem of insufficient waterproofing and dustproofing of traditional devices to ensure that information collection is not disturbed; (5) an intelligent fracture identification function is proposed to improve the efficiency and accuracy of rock fracture identification; and (6) a long-term unmanned continuous monitoring method is proposed to ensure the timeliness and continuity of rock mass information collection. The working temperature range of the device is −20 °C to 60 °C, and the traction force is 100 N, making it suitable for vertical borehole. Laboratory and field tests prove the stability and reliability of the device, which can support the long-term monitoring application of the deep rock mass project site, showing prefect performance and broad application prospects.

1. Introduction

To meet the development needs of the national economy, underground projects such as metal mines, transportation tunnels, and water conservancy and hydropower projects are undertaken at increasing depth [1-4]. The geological conditions of deep rock masses are highly complex and are often accompanied by the presence of high stresses. In the process of underground engineering excavation, due to the removal and destruction of rock, the surrounding stress field change, resulting in deformation and fracture of rock mass [5,6], which may lead to hazards such as rock bursts, spalling, and collapses. In particular, some hazards are time-dependent, do not occur immediately, but rather arise after a certain period of excavation or at a specific distance from the tunnel face. In such cases, staffs are often unprepared, leading to loss of life and property [7-10]. Therefore, there is an urgent need for systematic monitoring of rock mass information, in-depth analysis of its failure mechanisms and triggering processes, and the realization of more effective hazard prediction and early warning.

Monitoring deformation and fracture of rock mass is very essential for disaster prediction. Through monitoring the deformation and fracture characteristics of the rock mass, such as fracture propagation, stress concentration, and fault activity[11], potential disaster risks can be identified, including rock burst, collapse, lining, spalling and falling blocks. This provides an important basis for the design, construction and safety monitoring of underground engineering. Previously, many researchers employed various methods to obtain deformation and fracture information of rock masses. Multi-point displacement sensors, by deploying multiple sensors inside tunnel, can measure the changes in displacements at various depths in real-time. This allows for the monitoring of deformation processes of the surrounding rock mass[12,13]. Optical fiber sensors, when deployed in the borehole walls, utilize changes in the reflection of light signals transmitted through the optical fibers to monitor strain in real time. This allows for the detection of surrounding rock mass strain, providing valuable insights into the behavior of the rock mass during engineering

Peer review under responsibility of Editorial Board of of Deep Resources Engineering.
* Corresponding author at: State Key Laoratory of Intelligent Deep Metal Mining and Equipment, Northeastern University, Shenyang 110819, China.
E-mail address: zhaojun1@mail.neu.edu.cn (J. Zhao).

https://doi.org/10.1016/j.deepre.2025.100204
Received 12 May 2025; Received in revised form 1 July 2025; Accepted 7 July 2025
Available online 9 July 2025

excavation [14–17]. Microseismic monitoring technology captures low-energy seismic waves caused by the fracture activity in the surrounding rock mass. It accurately locates fractures and monitors their extension by analyzing the source location, frequency, and vibration characteristics in real time. This provides high-resolution data on the stability of the surrounding rock mass[18–22]. Monitoring of the wave velocity involves measuring the changes in the speed of propagation of sound or elastic waves through the surrounding rock mass. This helps to assess variations in fractures, porosity, and strength of the rock [23–27]. Borehole imaging technology uses optical imaging sensors to capture high-resolution images of the borehole walls inside tunnel. It allows intuitive and accurate identification of the distribution and evolution of fractures, providing detailed geological information [28–33]. The aforementioned techniques provide crucial data for those assessing the stability of the surrounding rock mass, offering support for risk management and support design in tunnel construction.

However, in rock mass information monitoring, optical fiber sensors and multipoint displacement gauges face challenges such as complex installation, high costs, environmental interference, and data processing difficulties. Microseismic monitoring technology cannot intuitively display the internal state of rock mass by monitoring the elastic wave generated by the stress change of rock mass. Borehole imaging technology demands high quality of the borehole wall, involves complex data processing, and cannot monitor fractures in deep engineering in real time. Furthermore, monitoring deformation and fractures in rock mass typically requires two borehole locations and multiple specialized personnel, rendering real-time monitoring impractical.

In this study, an intelligent device for simultaneous monitoring of deformation and fracture of boreholes in rock mass is designed specifically for engineering applications. The device featuring a high-performance mobile platform and a laser-videos based integrated probe, is capable of adapting to complex rock mass environments while capturing real-time data on borehole deformation, as well as fracture, characteristics such as direction, inclination, and with depth. Monitoring efficiency of rock mass is increased using intelligent algorithms for preliminary data analysis. The system comprises key components: the monitoring system, mobile platform, control system, power supply, and data analysis system. Functional validation through typical laboratory and field tests confirms its reliability.

2. Device components

Based on technological innovation and user feedback, the equipment has undergone three generations of iterations. The first generation device is characterized by a single track moving structure for fracture monitoring. The second generation upgrades the crawling structure and information acquisition sensors, improving performance. The third generation device integrates advanced technologies, enhancing its stability and intelligence, addressing the limitations of previous generations, and meeting more complex demands (Fig. 1 illustrates the evolution of the three generations of the device).

The third generation device is an integrated intelligent system for long-term continuous monitoring of internal deformation and fractures of boreholes in engineering rock mass. It is mainly composed of a controller, a cable drum, an extended sleeve and a crawling robot. These components are further combined to form multiple functional systems, including a crawling system, a monitoring system, a remote control and data analysis system (Fig. 1c). This device enables unmanned, long-term, automatic, and synchronized monitoring of deformation and fractures of boreholes in rock mass. It is also fully sealed with inflatable seals to prevent dust and water from entering the equipment within the borehole.

2.1. Crawling system

The crawling system consists of an adaptive main frame, upper and lower crawler transmission devices, and a drive motor (see Fig. 2). The upper and lower crawler transmission devices are mounted at the top

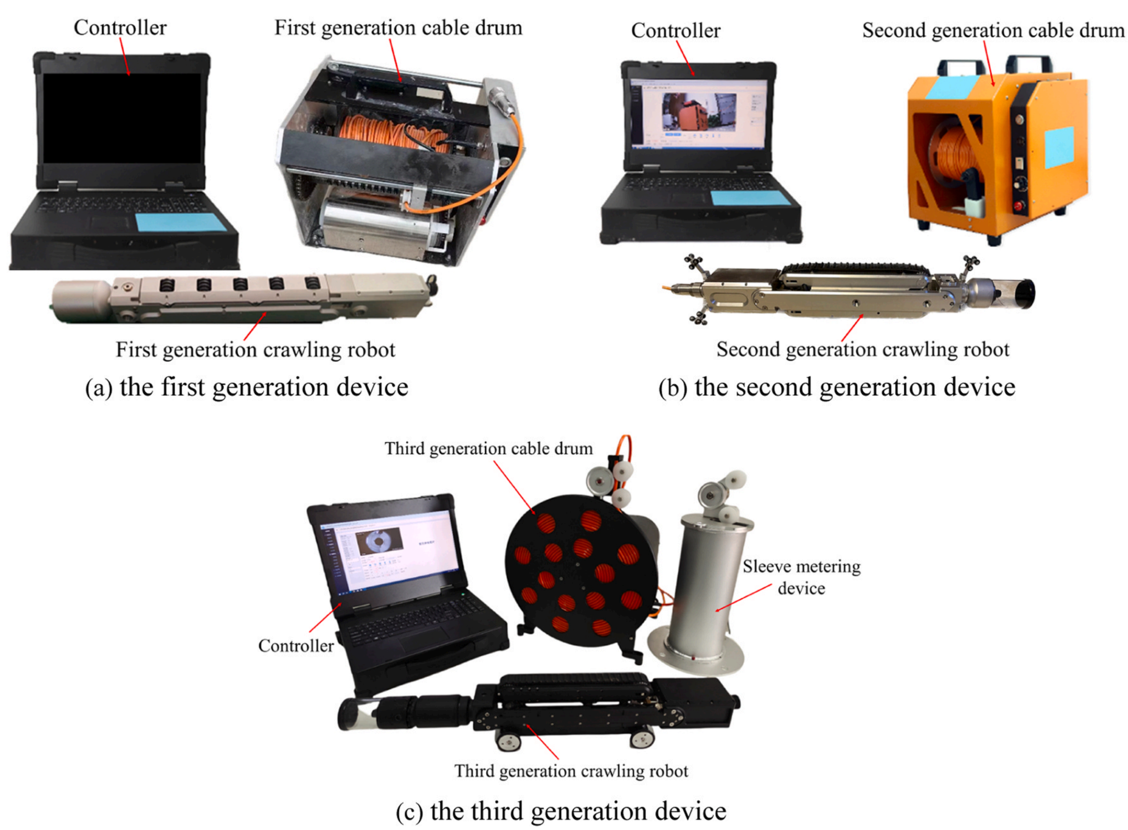

Fig. 1. An intelligent continuous monitoring device: (a) the single tracked monitoring device for hard rock fractures; (b) the dual tracked continuous monitoring device for hard rock fractures; (c) the dual track and wheeled integrated continuous monitoring device for hard rock deformation and fractures.

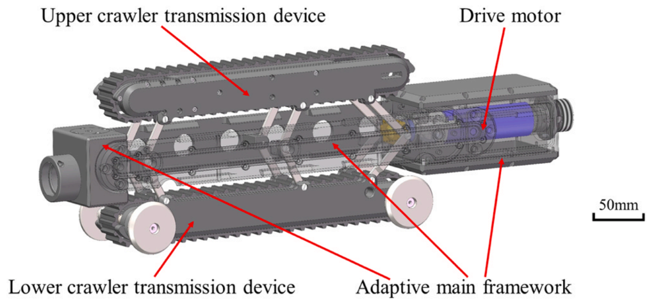

Fig. 2. The crawling mainframe of the integrated monitoring device.

and bottom ends of the main frame, while the drive motor is located at the rear of the main frame, which is responsible for controlling the unit's lifting by adjusting the rotation direction. The upper and lower crawler transmission devices are respectively equipped with a driving motor, and the power is transmitted to the upper and lower crawler units through the transmission mechanism to make the system move. Compared to the upper crawler transmission device, the lower crawler transmission device is additionally equipped with two sets of metal wheels, significantly enhancing the mobility and traffic capacity of the system in a complex geological environment.

2.2. Monitoring system

The monitoring system consists of an integrated laser-video probe, crawling distance monitoring device, air pressure sensor, attitude sensor, and tension sensor (Fig. 3). The integrated laser-video probe, located at the front of the crawling system, combines a high-definition fish-eye lens and a set of laser sensors to record rock mass morphology and perform contour scanning, enabling synchronously monitoring of rock deformation and fracture. The crawling distance monitoring device consisting of a primary cable drum counter and a secondary sleeve port counter, accurately tracks the equipment's crawling distance. The air pressure sensor installed within the device monitors the air pressure of the adaptive crawling robot in real time, reflecting the sealing condition. The attitude sensor measures the three-dimensional orientation (heading, pitch, and roll angles) of the equipment inside the borehole in rock mass, reflecting the three-dimensional direction of the borehole. The tension sensor monitors the reaction force received by the upper and lower crawler transmission devices to ensure that there is appropriate motivation to overcome the sliding resistance, ensure smooth movement inside a certain angle of boreholes in rock mass, and prevent slipping and jamming. Together, these monitoring devices form an integrated system that provides real-time data in the rock mass, ensuring the efficient operation of the crawling equipment and the accurate collection of information in boreholes.

2.3. Intelligent data analysis and remote control system

The data intelligence analysis system is a critical component of the device's software. It can preprocess and preliminary analyze the data collected by the monitoring system, providing easy to understand results that reduce the users' workload. The system processes the acquired video data to generate three-dimensional preview draws and a plane expanding images about the borehole, and enables the user to select any two points on the expanded image to calculate the distance between them to monitor the axial deformation of the rock mass. Additionally, the laser data can be used to create laser points cloud, simulating the internal morphology and deformation of the boreholes. The system also allows trajectories during boreholes monitoring to be recorded and displayed. In addition, the system also has online functions to support real-time data acquisition, transmission and back-end analysis to ensure efficient monitoring of rock mass information.

2.4. Performance parameters

The device was designed to enable remote monitoring of the internal morphology in rock mass and its internal deformation and fractures. Therefore, to achieve flexibility, reliability, and efficiency, certain requirements were imposed on the device parameters (Table 1). In addition, aspects of the technique need to be developed according to the required instrument parameters.

Table 1
Performance parameters of the intelligent continuous monitoring device for long-term deformation and fracture of borehole walls in engineering rocks.

Equipment functions	Technical parameters	Equipment functions	Technical parameters
Monitoring method	Simultaneous monitoring of deformation and fracture	Control method	Remote control
Crawling inclination	0 ~ 90°	Deformation measurement accuracy	0.1 mm
Operating temperature	−20 °C ~ 60 °C	Fracture recognition accuracy	0.1 mm
Waterproof rating	IP 68	Cable length	50 m
Hole size range	90 mm ~ 120 mm	Crawling traction	100 N

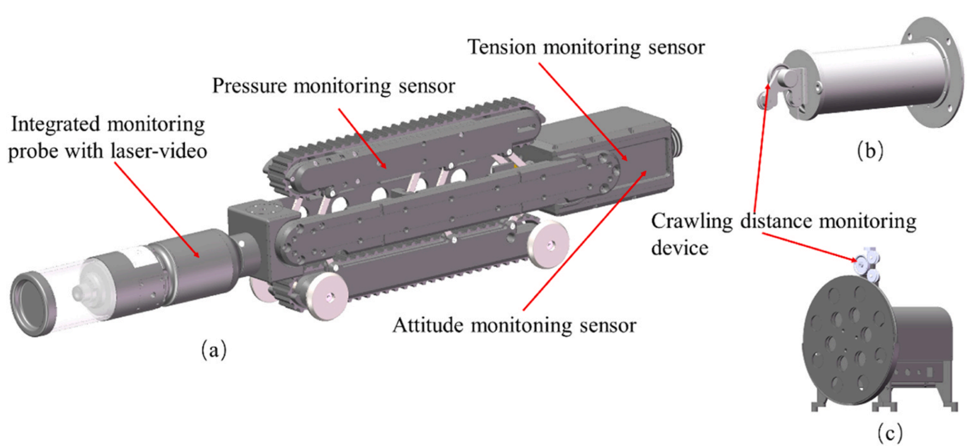

Fig. 3. Monitoring system layout diagram: (a) crawling rebot; (b) extended sleeve; (c) cable drum.

3. Key technologies

3.1. Wheeled-assisted tracked mobility units with variable diameter function

Traditional borehole imaging equipment collects fracture data using wheels subassembly. This design serves two purposes: it increases the distance between the probe and the borehole wall to prevent scrape induced by contact with debris from causing damage, and it shifts friction from sliding to rolling, reducing the operational load. However, the fixed size of wheels subassembly requires replacement to accommodate different borehole diameters. In rock mass, variations in on-site boreholes diameter often create gaps between the wheels subassembly and the borehole wall, leading to instability when passing through fracture zones or gravel layers. This instability results in image blurring, compromising the data quality and reducing the accuracy and reliability of fracture detection.

Fig. 4 demonstrates a schematic of the novel device designed for obstacle surmounting and continuous height adjustment. The device that utilizes upper and lower crawler transmission devices along with auxiliary wheels ensures smooth movement across complex terrain and maintains three-point contact with the borehole wall to prevent rollover. Its propulsion system combines upper and lower crawler with wheeled transmission. On the flat terrain, the lower track remains in a free state, unaffected by small obstacles. When traversing wide and deep fault zones, the device allows the lower crawler transmission device to engage with the fault zone edge, restoring traction and enabling smooth passage. The crawling power is generated by motors housed in the track cavity. The motors change the direction of the rotating shaft through the bevel gear mechanism, and then the gear group decelerates and increases the torsion. Finally, the power is transmitted to the track through the gear and belt system to ensure stable and efficient movement.

The device realizes automatic lifting through a multi-link mechanism. In Fig. 4b, points O, A, and B are located on the centerline of the device, and points A and B are fixed points that can only rotate. Point O can move and rotate along the centerline. The mechanism has one active component–connecting rod OI, the number of moving components $n = 9$, one moving pair, twelve rotating pairs, and low pair number $P_l = 13$. Therefore, the number of degrees of freedom $F = 3n - 2P_l - P_h = (3 \times 9) - (2 \times 13) - 1 = 1$, indicating that the mechanism can undergo definite relative motion. When the connecting rod OI moves to the right, the connecting rod OC, AF, BH rotates counterclockwise, and the connecting rod OD, AE, BG rotates clockwise, driving the long rod GEC downward and the long rod HFD upward, so as to realize the contraction of the device. When the OI moves to the left, the extension is implemented. The back-end servo motor realizes the movement of the top block at point O along the center line of the device through the screw drive (the left and right movement of the connecting rod OI). As shown in Fig. 5, the device can achieve seamless lifting adjustment between 90 mm and 130 mm.

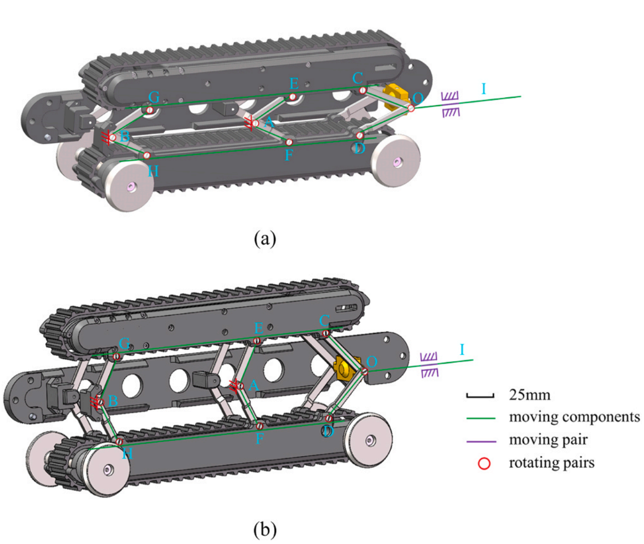

Fig. 4. Crawler lifting and lowering range: (a) schematic diagram of the general state of the device; (b) device schematic diagram of the structure during lifting.

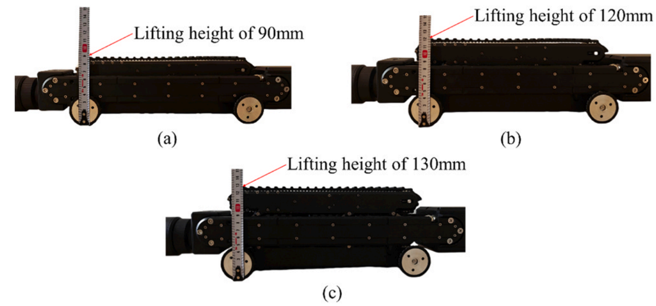

Fig. 5. The device lifted to different heights: (a) lifting height of 90 mm; (b) lifting height of 120 mm; (c) lifting height of 130 mm.

3.2. Laser-video rotatable integrated probe

Currently, fracture information of boreholes is collected using manually operated borehole imaging equipment, while the rock mass deformation needs to be measured by drilling additional boreholes nearby and installing multi-point displacement meter equipments. This method has high installation costs, heavy workload and requires professional technical support. Furthermore, since deformation and fracture information aren't collected from the same borehole, it is inaccurate to correlate two datasets for comparative analysis.

This study proposed a novel method to collect fracture information of boreholes using an image sensor and deformation information through laser sensors. To achieve the purpose, an acquisition probe integrating both sensors was designed, with the internal structure shown in Fig. 6. The probe comprises an electric rotating platform, a high-definition fish-eye lens, a set of high-precision laser ranging sensors, and a servo motor. The electric rotating platform consists of two sections: the front monitoring chamber and the rear power chamber. The front chamber houses the high-definition fish-eye lens and four laser ranging sensors, while the rear chamber contains the servo motor and control motherboard. The fish-eye lens is centrally located in the front chamber and is equipped with a halo light to ensure uniform illumination for clear imaging in dark conditions in boreholes. The laser ranging sensors are evenly distributed to form a surrounding array, ensuring complete environmental coverage. To prevent thermal damage, a gap is intentionally left between the lens and laser sensors for effective heat dissipation. The tail of the monitoring chamber features the hollow axle

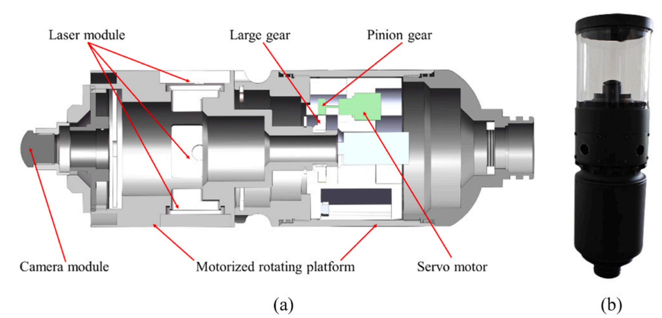

Fig. 6. Schematic diagram of the laser and video rotary integrated probe: (a) probe structure; (b) probe physical picture.

structure, with wiring routed through the hollow center to ensure the cleanliness and safety of the lines. The axle is securely coupled to the large gear via the keyway and fixed by an elastic ring to prevent gear displacement during operation. The servo motor, mounted eccentrically in the power chamber, drives the pinion through the keyway. The large and pinion gears are arranged in parallel to achieve relative meshing and stable power transmission. The servo motor rotates the pinion gear, which in turn rotates the large gear, thereby driving the monitoring chamber to rotate in a plane perpendicular to the large gear. This design allows the laser ranging sensors to perform 360° omnidirectional scanning within the borehole.

The design improves spatial utilization by eccentrically positioning the servo motor, thereby maintaining high performance within a compact environment. Integrating the image sensor and laser sensor enables the synchronous acquisition and comprehensive analysis of rock mass information from both monitoring technologies. Fig. 7 illustrates the real-time synchronized display of image and laser ranging data during the acquisition process.

3.3. High-precision meter counting system for boreholes

Combining borehole imaging and metering technology to achieve accurate positioning of borehole depth and key information is crucial to analyze the development mechanism of fracture. However, traditional manual equipment (such as tripod-based metering devices and hand-operated cable drum) requires multi-person and manual operation, often leading to cable extension beyond the metering range of the equipment and disconnection from the meter reading device, causing inaccuracy in image depth information. Additionally, the weight of the cable itself can make the metering results large, which makes the counting accuracy insufficient.

This study presents a high-precision borehole metering method and system. After drilling the rock wall, smoothing the borehole port, and installing the hollow extended sleeves with inner diameter matching the borehole to ensure concentricity (Fig. 8a). The sleeve serves both as the mounting base for the high-precision metering component and extends the device monitoring length, overcoming the limitation the information at the orifice cannot be monitored. Fig. 8b illustrates the structure of the extended sleeve. The opposite end of the sleeve is fitted with a cover plate, secured by rotatable bolts, can be opened and closed manually. When open, the device can be inserted or removed; when closed, it can not only carry out high-precision metering work, but also prevent the device from falling to the ground. High-precision electronic encoder is used in the metering device, and its accuracy is more than 3 times higher than that of the traditional device. The high-precision electronic encoder and two guide pulleys are arranged on the cover plate in a triangular arrangement, which increases the interaction force between the cable and the encoder wheel, reducing the error from the gravity of cable. To prevent cable misalignment and separation from the encoder, the guide wheel, encoder wheel, and cable outlet should be on the same plane. During data acquisition, the crawling robot drives the tail cable to move forward or backward. Due to the increase of the interaction force between the cable and the rollers, the counting error caused by the collapse of the cable under the action of gravity is reduced. The entire process is fully automated, minimizing human error and improving the precision of measurements.

In order to verify the accuracy of the measurement system, an indoor test platform was built and tested experimentally. Marks were made every 0.2 m, and the device was started to set the depth information to zero. The

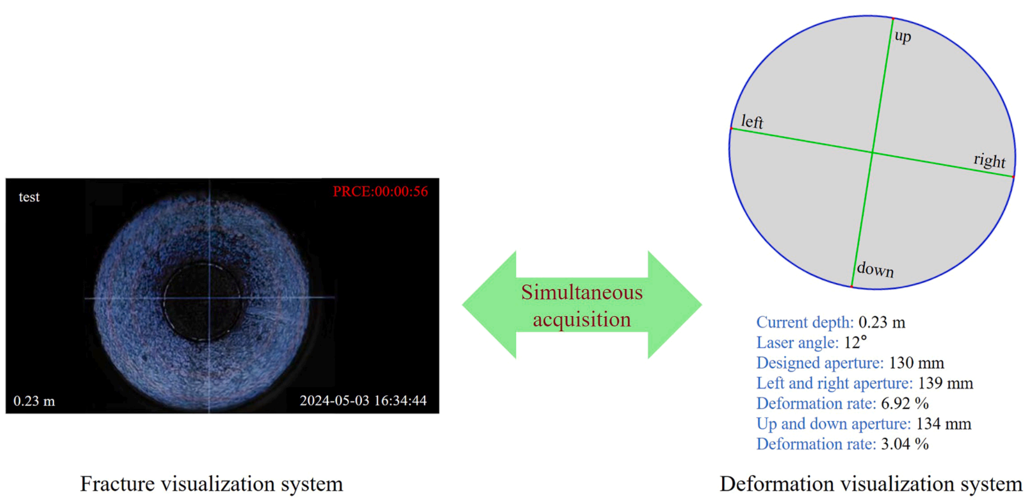

Fig. 7. Synchronized monitoring effect.

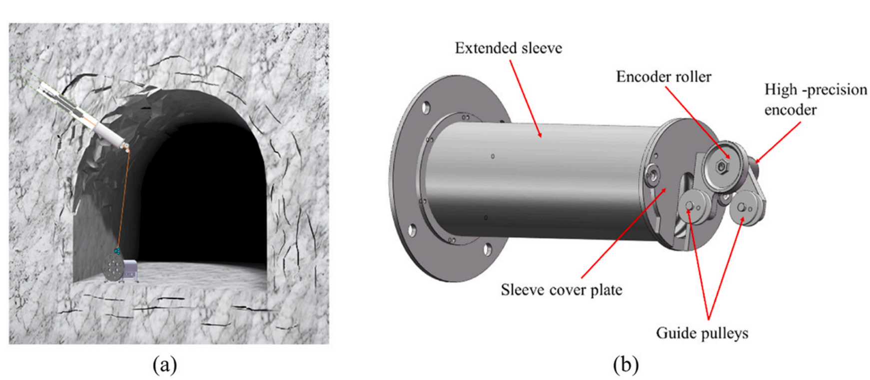

Fig. 8. The high-precision metering system: (a) installation of the high-precision metering system; (b) extended sleeve structure and high-precision metering system installation.

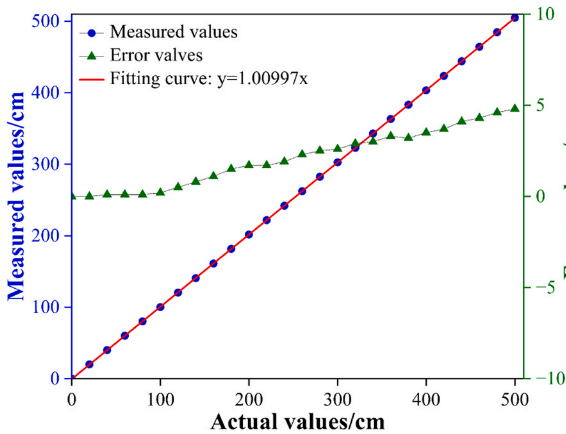

Fig. 9. Indoor measurement results of high-precision metering technology.

depth data could be recorded each time the crawling robot passed through the mark position. Measured results are shown in Fig. 9. In the test of 0–500 cm, the slope of the fitting curve between the measured values and the actual values is only 1.00997, and the maximum error is within 5 cm, suggesting that the accuracy of the system to measure the borehole depth reaches centimeter level, which can meet the needs of monitoring.

3.4. The sealed protection system

Considering the assembly of sensors and wiring, the housing design of the crawling robot adopts the semi-closed structure. To prevent the ingress of dust, moisture, corrosive gases, and other harmful substances, effective sealing solutions must be implemented to safeguard the sensors and wiring from malfunctions. Due to the variety in component design and connection methods, it is essential to select suitable sealing technologies to ensure the optimal protection and sealing integrity.

As shown in Fig. 10, the tail control chamber (Fig. 10b) and integrated probe (Fig. 10c) of the crawling robot are representative of the sealing

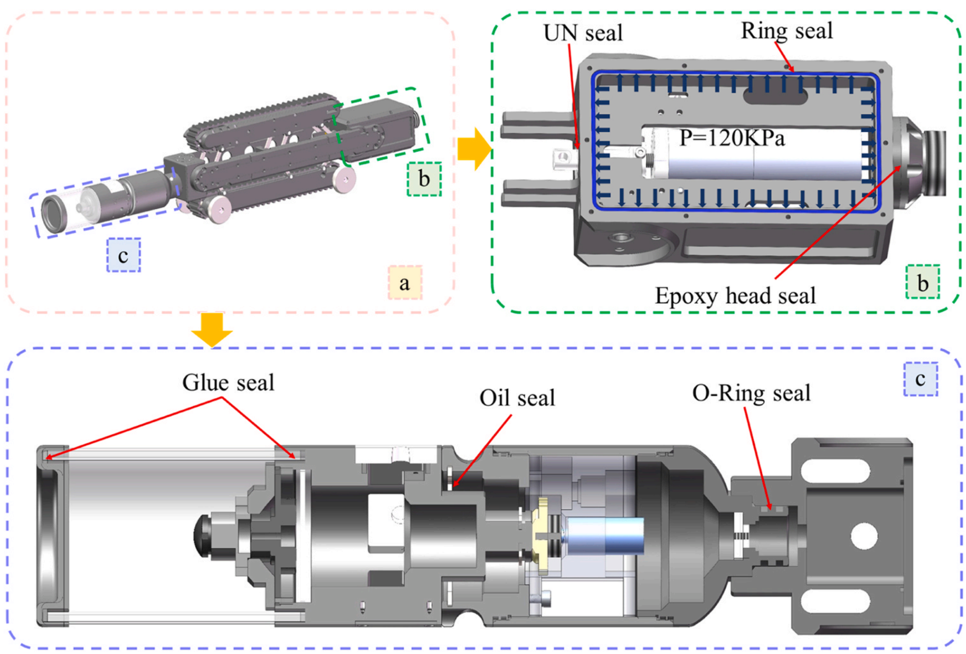

Fig. 10. Schematic diagram of the sealing: (a) partial view of device sealing; (b) control cavity sealing process; (c) integrated probe sealing process.

Fig. 11. Device watertightness test: (a) layout scheme; (b) immersion time and functional verification.

design of this device, which employs various forms of sealing methods. Taking into account the protection requirements and acquisition requirements, the front end of the image sensor uses a glass tube and a metal plug and is sealed with adhesive. The connection between the monitoring and the power chambers needs to rotate relatively, so the oil seal is used to seal it, which can prevent external pollutants from entering, reduce the friction between mechanical parts and prolong the service life. In the integrated probe (Fig. 10c), considering facilitative transportation, the probe and frame are designed as a detachable structure, with axial fixation provided by double O-rings and a locking mechanism, preventing loosening due to vibration or impact. The tail control chamber (Fig. 10b) features an upper and lower opening structure for ease of motor and motherboard installation, sealed with high-performance rubber rings and multiple bolts to maintain constant air pressure and prolong component lifespan. The end of the control chamber is sealed with an epoxy resin head, with the core seat fastened by bolts; the resin's superior adhesion and corrosion resistance prevent leakage, while the bolts enhance sealing and connection strength. The front end of the control chamber includes a push rod control device, sealed with a UN ring and threaded fixed seat to reduce friction, improve motion efficiency, and adapt to dynamic conditions.

Through the comprehensive application of various sealing technologies, the reliability of the equipment in complex environments is ensured. As shown in Fig. 11, the equipment was submerged in a water tank at a depth of 500 mm for watertightness testing. Functional tests were performed at 30-minute intervals throughout the immersion period, with results recorded. After six hours of continuous submersion, the equipment was removed, and external surfaces were dried. Subsequent inspection revealed no internal moisture ingress or functional anomalies. These results confirm the equipment achieves its specified waterproof requirements.

3.5. Intelligent fracture-recognition technology

Traditional monitoring of fracture information relies on manual visual inspection and recording, which requires multiple data collection and line-by-line depiction. The number of borehole fracture is large and the workload is onerous when the conditions in rock mass are poor; this leads to inefficient recognition and frequent omissions.

Therefore, to improve datas processing speed and accuracy, the function of intelligent fracture-identification was introduced. The

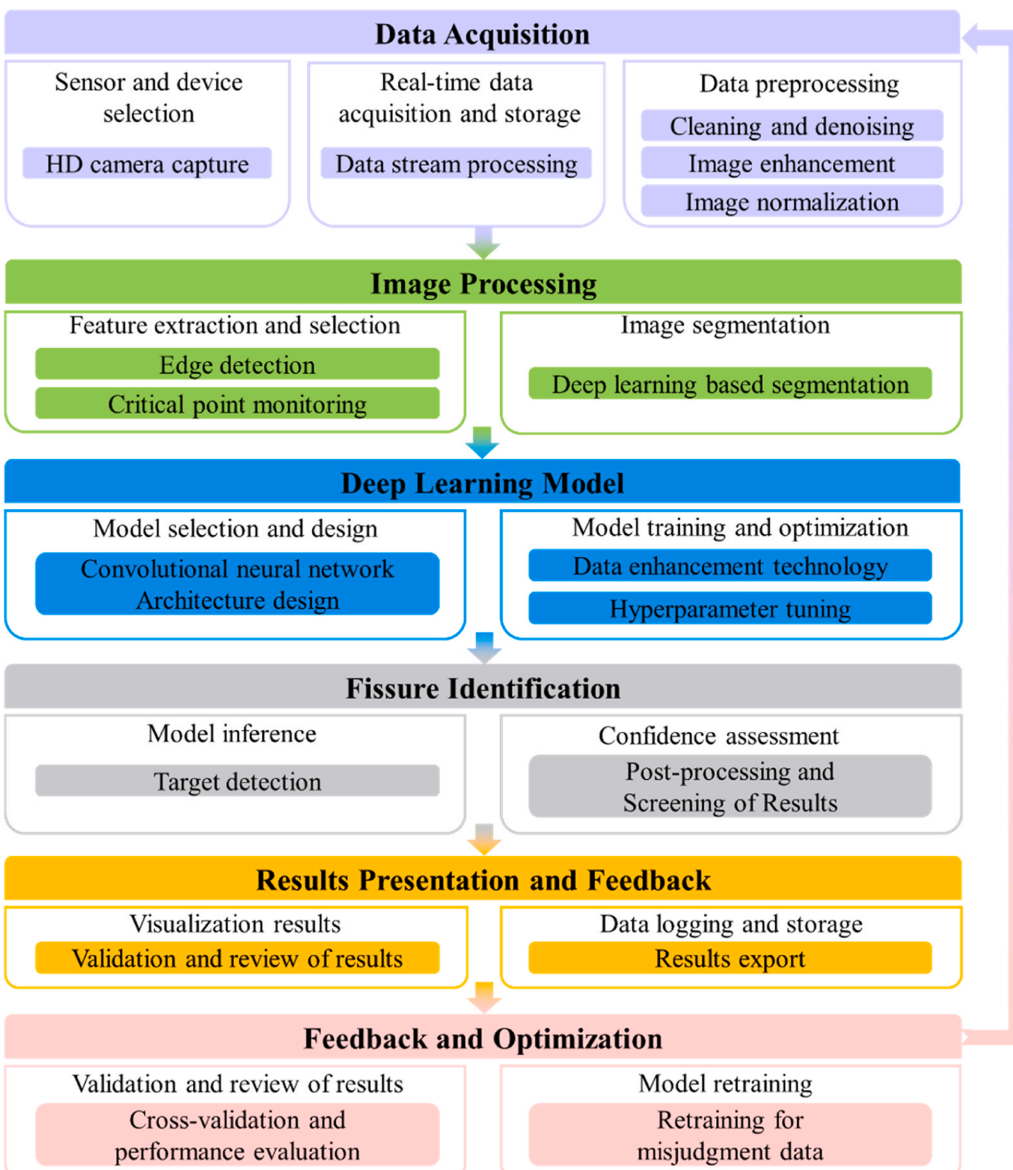

Fig. 12. Flowchart of the fully automated fracture recognition technique.

technical principle is shown in Fig. 12.

Firstly, the image data captured by the high-definition camera sensor is preprocessed: erroneous and redundant data caused by sensor noise and transmission interference is eliminated. And the image noise is eliminated by Gaussian filtering and median filtering to improve the image quality. Then, the image is normalized: the parameters such as brightness and contrast are adjusted to ensure the consistency of the images in subsequent processing. Next, accurately extracting edge features from images by edge detection algorithm, and using the key point detection technology to mark the representative feature points in the image to assist further fracture analysis. Afterwards, training the deep learning model by the convolutional neural network architecture according to the data characteristics. In the process of model training, the training data set is expanded by adjusting the number of iterations and data augmentation techniques, which improves the generalization ability of the model and optimizes the performance of the model. After the model training is completed, the preprocessed and feature-extracted images are input into it, and the model identifies the existence, location and type of fracture through inference. In order to ensure the accuracy of the results, the confidence of the prediction results is evaluated, and the results with high confidence are retained by setting a threshold. Finally, the fracture location and fracture type are marked with different colors, and the visualization results are output and exported to the folder. Moreover, by manually comparing the recognition result with the actual situation, misjudged or omitted data are fed back to the model for retraining and optimization, and the recognition speed and accuracy of the system are continuously improved.

To improve the accuracy of model recognition, the real fracture data collected on site were used as training samples (Fig. 13a). As shown in Fig. 13b, after more than 500 rounds of training, the recognition accuracy of the model has exceeded 95%.

3.6. Long-term unmanned monitoring technology

In deep engineering, monitoring of fracture changes and development of boreholes in rock mass currently requires the connection of multiple long rods to move the monitoring equipment through the boreholes. This is conducted collaboratively by at least two staffs to

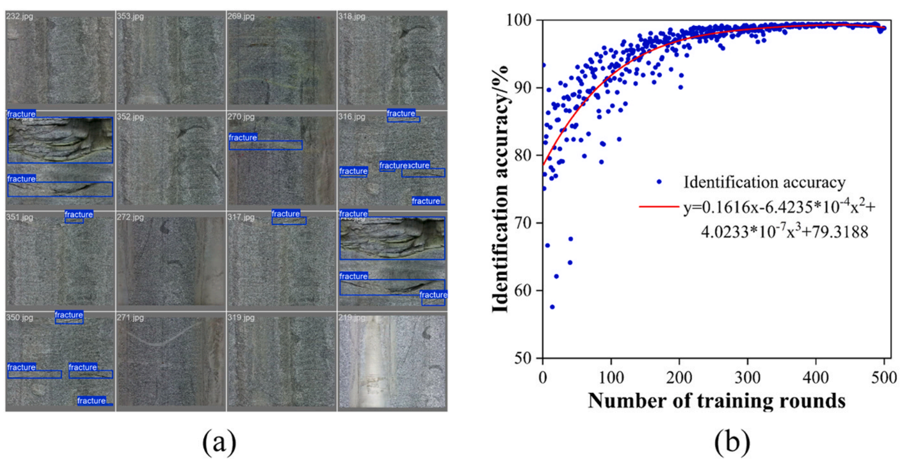

Fig. 13. Training process of smart identification of fractures: (a) training samples; (b) training results.

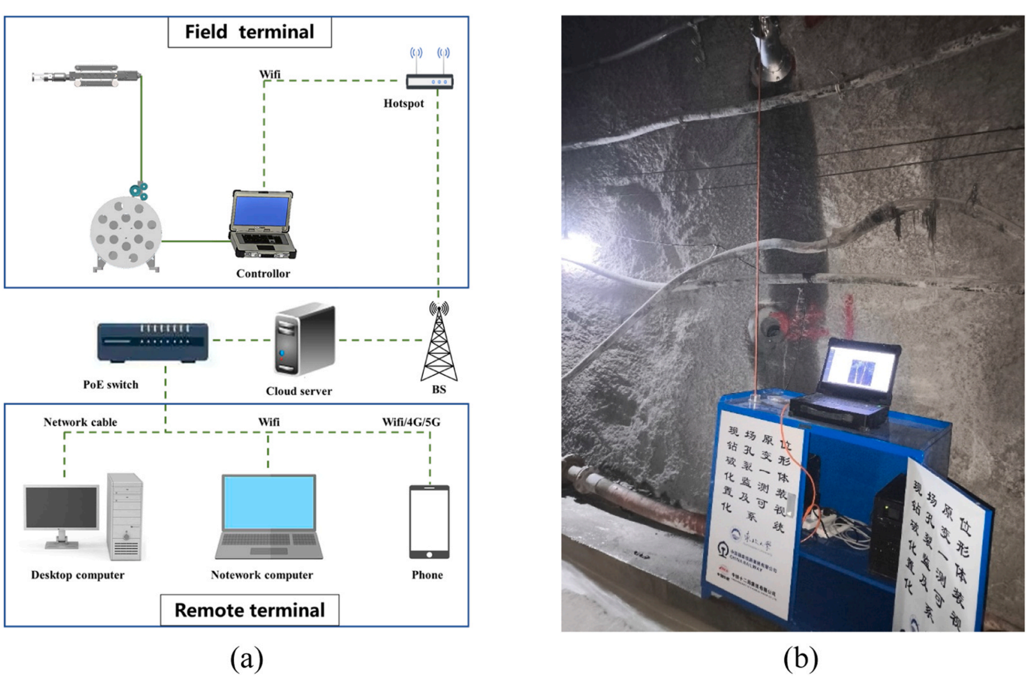

Fig. 14. Schematic diagram of the monitoring methodology: (a) schematic diagram of the monitoring methodology; (b) performance in timed acquisition tasks.

obtain complete information pertaining to the rock surrounding. In addition, during engineering blasting, the relevant personnel need to be evacuated from the scene for safety reasons, making it difficult to collect data in the first place. Intermittent data collection may miss key information in the process of rock mass disaster gestation, resulting in inadequate mechanism analysis.

The equipment uses long-term unmanned monitoring technology to continuously monitor the target area, reduce manual intervention, and improve monitoring efficiency and data accuracy. It adopts the integrated processing mode, integrates the functions of data acquisition, real-time display, data storage, and intelligent analysis in the controller, and is equipped with wireless network module to realize real-time control, monitoring, and data transmission. The equipment realizes the goal of automation, intelligence, and unattended monitoring by regularly starting and stopping the acquisition program. Meanwhile, the equipment is powered by the AC-DC power supply in the cable drum, and the external uninterruptible power supply (UPS) ensures its stable operation for 24 h to meet long-term monitoring requirements. The use process of the device is as follows: first, each component is arranged in an appropriate position, and the crawling robot is installed in the borehole and adjusted to a suitable height to ensure that it can move smoothly and collect data smoothly; then, the daily data acquisition time is set, and the operator can evacuate the scene at this time. Then, the device will automatically start at a predetermined time to start the collection of deformation information and fracture information; finally, after data acquisition is completed, the device will return to the starting position and transmit the collected data to the controller and the cloud in a good network environment (the data transmission diagram is shown in Fig. 14a).

The device effectively solves the problems of personnel safety risks and discontinuous data collection in traditional monitoring methods by means of long-term unmanned monitoring technology. Through real-time monitoring and automatic data logging by the intelligent system, the device is capable of continuously and stably collecting and transmitting critical data without human intervention, while ensuring that the monitoring process is efficient and accurate. Meanwhile, the system is also equipped with autonomous diagnostic and fault warning functions, which further improve the safety and reliability of the monitoring process. Fig. 14b shows the device performing a timed acquisition task.

4. On-site monitoring results

4.1. Preparation for monitoring

A deeply buried tunnel in Southwest China is located in a Y-shaped tectonic zone which is characterized by extremely high tectonic stresses and complex geological structures. The tunnel had frequent rock bursts during the previous construction phase, including continuous strong rockbursts and long time-delayed rockbursts. In order to research the sudden hazards in the tunnel and ensure the construction safety, stability monitoring was carried out.

In rock mass monitoring, multiple monitoring boreholes are arranged to collect data from different directions, improve spatial coverage, avoid the accident of single borehole monitoring, and ensure that comprehensive changes in surrounding rock characteristics are monitored. As shown in Fig. 15a, three monitoring boreholes are arranged in the same section of the tunnel: #1borehole is 3 m long, 2° downward tilt, 1.5 m from the ground; #2 borehole is 10 m long, and 6° upward, 3 m above the ground. They are arranged on the right side of the section. #3 borehole is 3 m long, located on the left-hand side of the section, 2 m above the ground, and 4° downward.

This layout reduces the deviation caused by geological heterogeneity and instrument error through multi-angle cross-validation, and enhances the reliability of data. Before monitoring, the orifice needs to be treated first to ensure the requisite level and provide a stable foundation. Then, the extension sleeve is installed in the orifice and bolted in place.

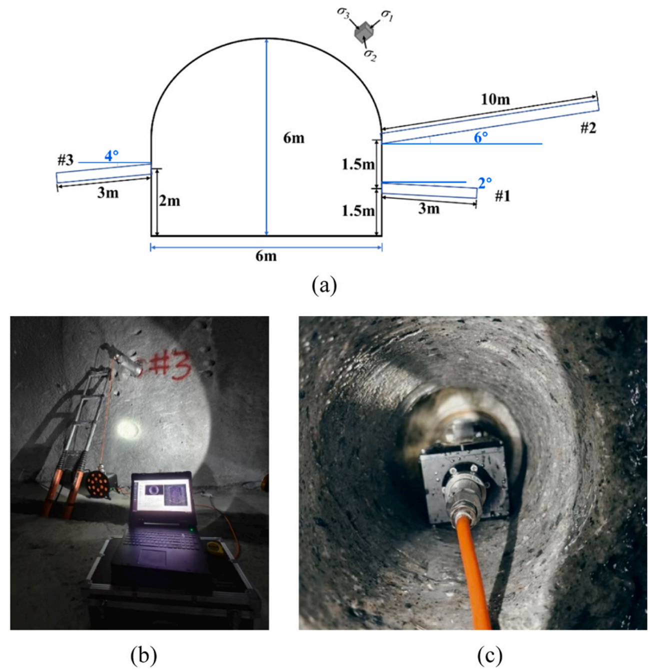

Fig. 15. The on-site boreholes and equipment layout: (a) the arrangement of monitoring boreholes on site; (b) the on-site borehole layout; (c) the equipment is working in the borehole.

Placing the device into the sleeve and cable drum should be placed under the instrument to facilitate subsequent connection. Each device is then connected in turn and the power supply activated to ensure proper operation of the system (Fig. 15b). In this process, it is necessary to control the length of the cable to ensure the smooth installation of the crawling robot and avoid redundant cables interfering with instrument operation. After all installations are completed, the operators check whether the equipment is operating normally, and start data acquisition after confirming that it is correct. This process ensures the accuracy and reliability of monitoring rock mass information, and provides high-quality raw data support for subsequent analysis. Fig. 15c shows the crawling robot during information monitoring task.

4.2. Monitoring results

4.2.1. Deformation monitoring

Fig. 16 illustrates the point cloud profile of #1 borehole obtained by laser scanning technique. It can be seen from the figure that the depth of #1 borehole is 3,200 mm, and the overall profile is close to circular. The profile at the orifice is more prominent than the rest of the borehole, and it is speculated that a wide fracture zone may exist in this zone. This conjecture was verified using the borehole imaging device. The result confirms that there is indeed a wide fracture zone at the orifice, indicating that the rock structure is looser or severely fractured in this area. Meanwhile, the point cloud data shows that the center and inner regions of the borehole are relatively flat, with no obvious structural anomalies or signs of fracture.

To quantify the radial deformation of the borehole, 500 mm, 1,500 mm, and 2,500 mm were selected as reference depths and compared with the standard borehole diameter to identify the anomalies of the borehole in all directions. As shown in Fig. 17a-c, the gray square dots represent the profile with the standard aperture of 130 mm, the blue dots represent the measurement data in April, and the red triangle dots represent the measurement data in May. The scanning data of different reference depths shows that the profiles at depths of 500 mm and 1,500 mm are more regular, indicating that the geological conditions are better and the damage is less extensive. At the depth of

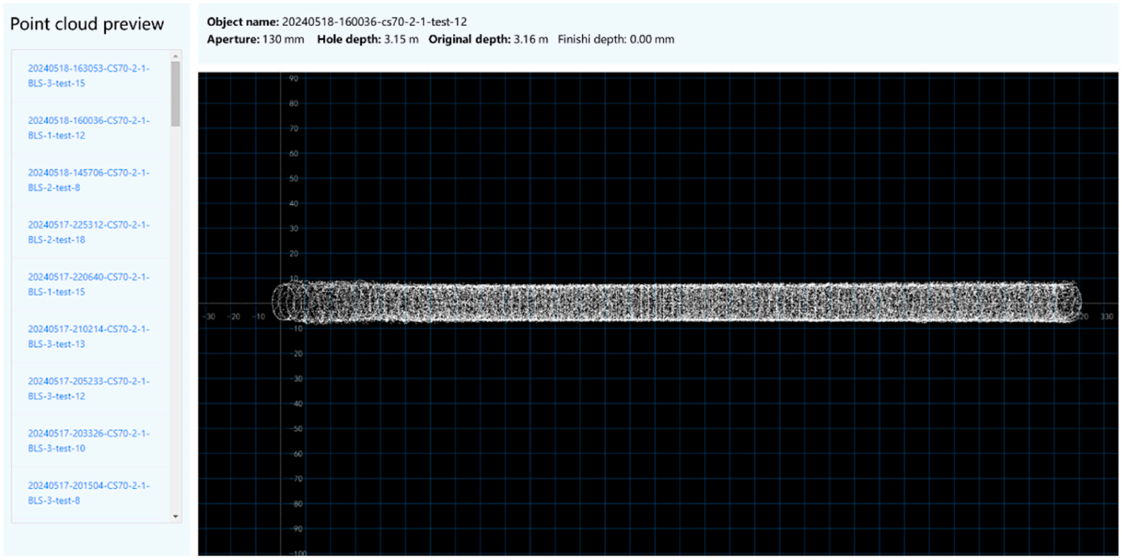

Fig. 16. Results of the complete scan of the borehole wall profile.

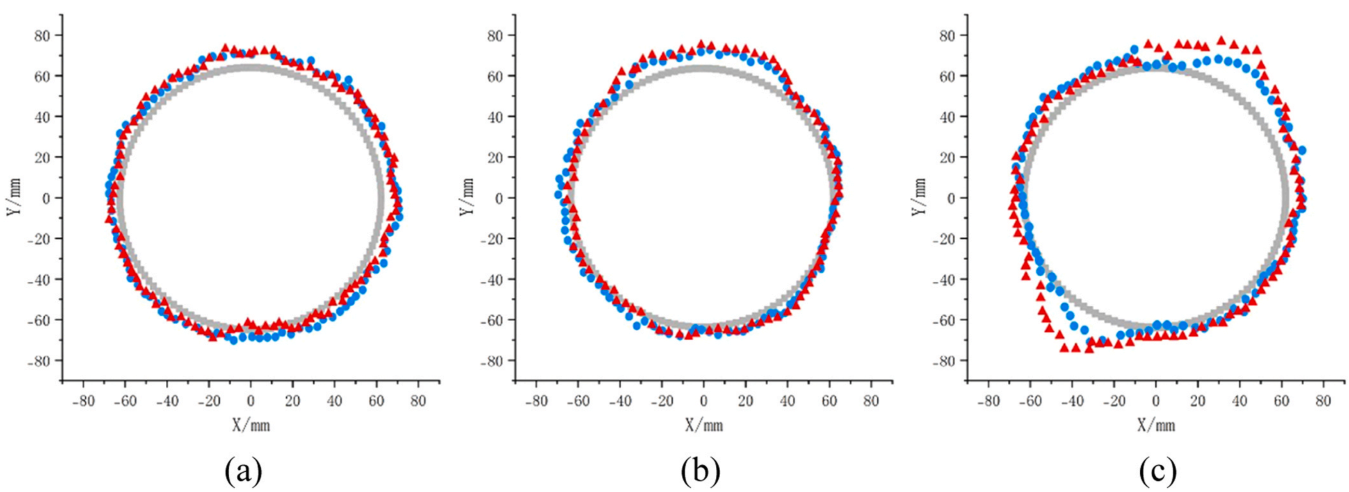

Fig. 17. Comparison of deformation data collected at different time points at the same reference depth: (a) reference depth of 500 mm; (b) reference depth of 1,500 mm; (c) reference depth of 2,500 mm.

2,500 mm, the profile shows obvious anomalies, especially the significant uplifts in the upper right and lower left corners (at an angle of about 180°), which may indicate the presence of the fault zone.

Further analyzing the scanning data at the same reference depth at different times revealed that the concave appeared below the cross-section contour at the depth of 500 mm, and there was no significant change in other areas. It is speculated that there may be debris or foreign bodies therein. The protrusions above the section at a depth of 1,500 mm increase significantly, indicating that the upper fracture surface expands, which may be caused by the displacement of loose rock. At a depth of 2,500 mm, the anomaly is more significant, the convex area in the upper right corner tends to be stable, while the convex area in the lower left corner increases significantly, the width and height increase, but the angle between the two changes little and remains quasi-stable. Therefore, it is speculated that these two cracks propagate in the circumferential direction.

4.2.2. Fracture monitoring

Fig. 18 illustrates the image information acquired by the equipment on May 3 and 12 in borehole #2. The images obtained from both data acquisitions are of high quality, with clear, sharp image colors, smooth stitching process, and no image interference such as blurry stripes; the positions of the features in both the front and rear images can be accurately aligned, ensuring the consistency and reliability of the data. The comparison of these two sets of data revealed two new fractures at the fracture in the front of the borehole zone. Meanwhile significant development and extension of pre-existing fractures appear in the central part of the borehole. These fracture changes are clearly observed in the images, providing great convenience for further analysis. In order to obtain the detailed information of the fracture change, the plane dimensions of the fracture were measured using the accurate in the

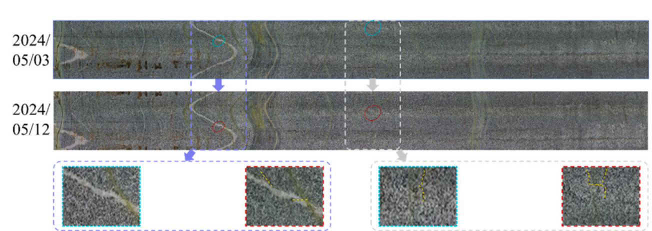

Fig. 18. Image information of Borehole #2.

software. Measurements indicate that the dimensions of the two nascent fractures are 26 mm and 31 mm, respectively. These data may provide a quantitative basis for subsequent geological assessment.

4.2.3. Other monitoring

Fig. 19 illustrates the comparison of the depth measurement of #2 borehole by the traditional instrument counting device and the high-precision metering device. The measurement starts from the same starting point and ends at the same point. The traditional equipment measured the depth of 7.7 m, while the high-precision device measured the depth of 7.0 m. To verify the accuracy, measurements was performed using the laser rangefinder and the result was also 7.0 m. The values measured using the high-precision device were thus deemed consistent with those measured by laser range-finder, evincing the precision and reliability of the proposed device. In contrast, the measurement results of traditional equipment (7.7 m) deviated from these data. This comparison verifies the superiority of the high-precision metering device for measuring the borehole depth.

Fig. 20 shows the entire trajectory recorded by the device when collecting information on #3 borehole. By accurately measuring and recording the motion trajectory, the device can draw the specific motion path in the three-dimensional coordinate system, comprehensively analyze the geological environment around borehole. To present the borehole direction in a more intuitive way, the right of the figure shows the offsets in the east-west, north-south, and vertical directions. The high accuracy of data recording was verified by comparing the data with the three-dimensional spatial data arising from the electronic magnetometer and 3D laser scanner. These offset data clearly reflect the changes of boreholes in different directions, which helps researchers to understand the actual process of borehole advancement and the precise location thereof in the complicated underground environment.

Fig. 21 illustrates the results of intelligent recognition of fracture in image information collected in boreholes at the project site. Fig. 21a shows the original plane expansion diagram, while Fig. 21b demonstrates the image information after automatic identification and analysis. All fracture zones have been marked and confidence information is shown. The confidence levels of all labels are high, indicating that the recognition process is both accurate and reliable.

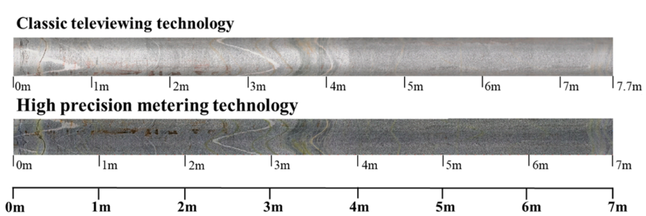

Fig. 19. Comparison of depth measurement results between the two devices.

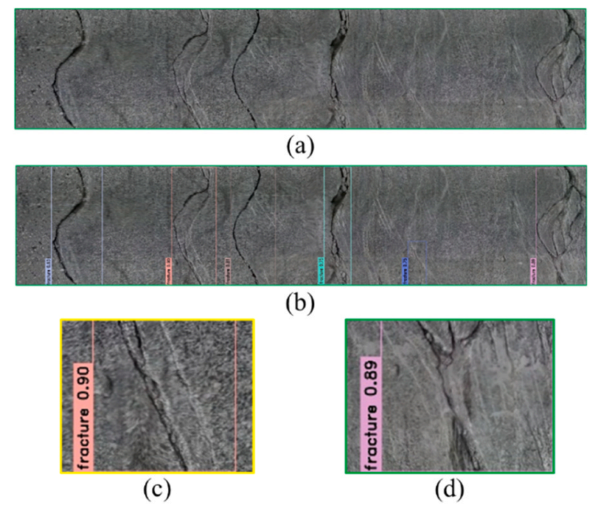

Fig. 21. Smart identification technology of fractures: (a) routine fracyures acquisition results; (b) smart recognition results; (c-d) local amplification diagrams of smart recognition information.

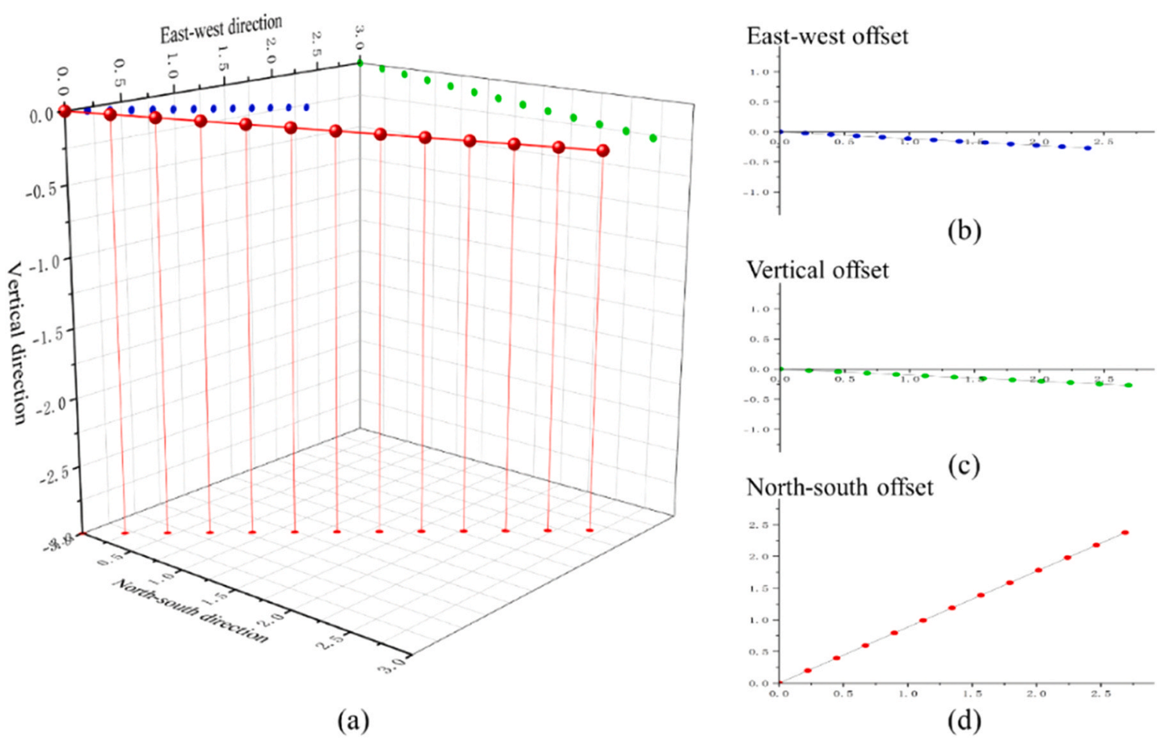

Fig. 20. Display of the device trajectory: (a) three-dimensional preview of the equipment motion trajectory; (b) the east-west offset; (c) the vertical offset; (d) the north-south offset.

5. Conclusions

A novel integrated intelligent monitoring device for deformation and fracture has been developed. It can be used under complex conditions and overcome the difficulties in the development of borehole monitoring technology at engineering sites. This paper includes description of the structure and function of the monitoring device, discusses advances in key technologies and performance data. The performance and reliability of the device were verified through a series of laboratory tests as well as *in-situ* applications on engineering sites. The following conclusions can be drawn:

(1) The device designed has great adaptability, which can be able to move smoothly in boreholes with a dip angle of 0° to 90° and a diameter of 90 mm to 130 mm. Its structural design ensures that the device can smoothly pass through areas of broken rock, fully meeting the needs of operation in complex geological environments. Meanwhile, the unit has excellent sealing performance and maintains normal operation even when operating under water. In addition, it is easy to operate and only one staff is required to complete the related work of rock mass information collection, which greatly improves the operational efficiency.

(2) The equipment enables advanced synchronous acquisition of rock mass deformation and fracture information. It is capable of displaying high-definition images and point cloud contours of the interior of boreholes, providing reliable data support for accurate geological analysis. Meanwhile, the device is equipped with intelligent data analysis. It can automatically identify and label the key fracture information in boreholes, thus improving the efficiency of analysis and processing of fracture information. The device also supports real-time recording of movement trajectories to ensure complete traceability of the acquisition process. The combination of these features allows the device to increase the working efficiency and enhance the intelligence of the operating process.

(3) The device is equipped with a remote control and remote data transmission function. Researchers, contractors, engineers, as well as geologists do not need to be physically present on site, significantly reducing the intensity of their work and potential risks to their safety. In addition, the continuity and timeliness of information acquisition is ensured through the combination of timed automatic acquisition and remote-controlled acquisition. These provide complete and comprehensive data support for predicting the occurrence mechanism and evolution of disasters in deep rock mass engineering.

CRediT authorship contribution statement

Jun Zhao: Writing – review & editing, Supervision, Software, Methodology, Investigation, Funding acquisition, Conceptualization. **Jiang-Long Zhao:** Writing – original draft, Visualization, Validation, Software, Investigation, Data curation. **Xia-Ting Feng:** Supervision, Resources, Project administration, Methodology, Funding acquisition, Formal analysis. **Yue Guo:** Writing – review & editing, Validation, Supervision, Methodology, Conceptualization. **Xiao-Jun Zhang:** Visualization, Software, Investigation, Data curation. **Hong-Wei Xiang:** Methodology, Investigation, Conceptualization.

Declaration of Competing Interest

The authors declare that they have no conflicts of interest.

Acknowledgments

The authors gratefully acknowledge financial support from the National Natural Science Foundation of China (Grant No. 52209125) and the Department of Science and Technology of Liaoning Province (Grant No. 2025JH6/101000011). We are also particularly grateful for the kind assistance provided by Mr. Mengfei Jiang, Mr. Chen Fan and Mr. Lei Wang.

Data availability statement

All data included in this study are available upon reasonable request by contact with the corresponding author.

References

[1] Y.X. Xiao, X.T. Feng, S.J. Li, et al., Rock mass failure mechanisms during the evolution process of rockbursts in tunnels, Int. J. Rock Mech. Min. Sci. 83 (2016) 174–181.
[2] R. Patyńska, K. Stec, The seismic activity of mines in the Upper Silesian Coal Basin and rockburst hazard in the years 2001–2015, Zesz. Nauk. Inst. Gospod. Surowcami Miner. Pol. Akad. Nauk. 97 (2017) 135–144.
[3] A. Mahdi, S. Ali, R. Alain, et al., Rockburst in underground excavations: A review of mechanism, classification, and prediction methods, Undergr. Space 7 (4) (2022) 577–607.
[4] J.Q. Lin, X.Q. Fang, J.L. Liu, Earthquake damage evaluation of tunnels, Appl. Mech. Mater. 1800 (170–173) (2012) 1402–1409.
[5] J. Zhao, X.T. Feng, C.X. Yang, et al., Study on time-dependent fracturing behaviour for three different hard rock under high true triaxial stress, Rock Mech. Rock Eng. 54 (3) (2021) 1239–1255.
[6] X. Zhang, G.Y. Si, Q.S. Bai, et al., Numerical simulation of hydraulic fracturing and associated seismicity in lab-scale coal samples: A new insight into the stress and aperture evolution, Comput. Geotech. 160 (2023) 105507.
[7] C. Fan, X.T. Feng, L.J. Fu, et al., Evolution law and mechanism of time-delayed spalling in a deep TBM tunnel: A case study, Eng. Geol. 325 (2023) 107309.
[8] J. Zhao, X.T. Feng, H.S. Guo, et al., Time-dependent failure characteristics of excavated rock masses in deep buried engineering: A field case and experimental study, Bull. Eng. Geol. Environ. 81 (2022) 520.
[9] S.Y. Wang, G.Y. Si, C.B. Wang, et al., Quantitative assessment of the spatio-temporal correlations of seismic events induced by longwall coal mining, J. Rock Mech. Geotech. Eng. 14 (5) (2022) 1406–1420.
[10] G.L. Feng, Q. Ma, G. Lacidogna, et al., Experimental study on the failure characteristic and mechanism of granite time-delayed rockburst under true triaxial condition, Geomech. Geophys. Geo-energ. Geo-resour. 9 (2023) 164.
[11] S.Y. He, Experimental study of crack propagation law of shale containing prefabricated fractures, Adv. Civ. Eng. Mater. 7 (1) (2018) 558–575.
[12] D. Lydon, M. Lydon, J.M. del Rincón, et al., Development and field testing of a time-synchronized system for multi-point displacement calculation using low-cost wireless vision-based sensors, IEEE Sens. J. 18 (23) (2018) 9744–9754.
[13] X.T. Feng, Z.B. Yao, S.J. Li, et al., In situ observation of hard surrounding rock displacement at 2400-m-deep tunnels, Rock Mech. Rock Eng. 51 (3) (2018) 873–892.
[14] K. Soga, L.Q. Luo, Distributed fiber optics sensors for civil engineering infrastructure sensing, J. Struct. Integr. Maint. 3 (1) (2018) 1–21.
[15] C.S. Wu, Z.Y. Feng, H. Yang, et al., Evolution mechanism of rock slope slide based on fiber optic sensors, J. Nanoelectron. Optoelectron. 12 (9) (2017) 913–919.
[16] Y. Zheng, D.Y. Liu, Z.W. Zhu, et al., Experimental study on slope deformation monitoring based on a combined optical fiber transducer, J. Sens. 2017 (2017) 7936089.
[17] W. Lee, W.J. Lee, S.B. Lee, et al., Measurement of pile load transfer using the fiber bragg grating sensor system, Can. Geotech. J. 41 (6) (2004) 1222–1232.
[18] D. Anikiev, C. Birnie, U. bin Waheed, et al., Machine learning in microseismic monitoring, Earth-Sci. Rev. 239 (2023) 104371.
[19] B.R. Chen, X.T. Feng, Q.Q. Fu, et al., Integration and high precision intelligence microseismic monitoring technology and its application in deep rock engineering, Rock Soil Mech. 41 (7) (2020) 2422–2431.
[20] F. Liu, Y. Wang, M.M. Kou, et al., Applications of microseismic monitoring technique in coal mines: A state-of-the-art review, Appl. Sci. 14 (4) (2024) 1509.
[21] Z.L. Zhou, C.C. Zhao, Y.H. Huang, An optimization method for the station layout of a microseismic monitoring system in underground mine engineering, Sensors 22 (13) (2022) 4775.
[22] N.W. Xu, T.B. Li, F. Dai, et al., Microseismic monitoring of strainburst activities in deep tunnels at the Jinping II hydropower station, China, Rock Mech. Rock Eng. 49 (3) (2016) 981–1000.
[23] S.J. Chen, Z.G. Zhu, Y. Zhao, et al., Numerical simulation and parametric analysis of ultrasonic velocity test in fractured rock based on the discrete element method, Rock Mech. Rock Eng. 57 (10) (2024) 8563–8579.
[24] L. Liu, S.J. Li, M.Z. Zheng, et al., Inverting the rock mass P-wave velocity field ahead of deep buried tunnel face while borehole drilling, Int. J. Min. Sci. Technol. 34 (5) (2024) 681–697.
[25] L. Liu, S.J. Li, M.Z. Zheng, et al., Identification of rock discontinuities by coda wave analysis while borehole drilling in deep buried tunnels, Tunn. Undergr. Space Technol. 153 (2024) 105969.
[26] S.Y. Peng, X.B. Li, C.J. Li, et al., Crack-closure behavior and stress-sensitive wave velocity of hard rock based on flat-joint model in particle-flow-code (PFC) modeling, Comput. Geotech. 170 (2024) 106320.

[27] X. Li, G.Y. Si, J. Oh, et al., A pre-peak elastoplastic damage model of Gosford sandstone based on acoustic emission and ultrasonic wave measurement, Rock Mech. Rock Eng. 55 (8) (2022) 4819–4838.
[28] S.J. Li, X.T. Feng, C.Y. Wang, et al., ISRM suggested method for rock fractures observations using a borehole digital optical televiewer, Rock Mech. Rock Eng. 46 (3) (2013) 635–644.
[29] Z.Q. Han, C.Y. Wang, H.Y. Zhu, Research on deep joints and lode extension based on digital borehole camera technology, Pol. Marit. Res. 22 (s1) (2015) 10–14.
[30] Y.Z. Zhang, H.G. Ji, W.G. Li, et al., Research on rapid evaluation of rock mass quality based on ultrasonic borehole imaging technology and fractal method, Adv. Mater. Sci. Eng. 2021 (2021) 8063665.
[31] R. Dashti, B. Birt, M. Jangani, Quick structural modelling using multi-hole borehole image analysis; a critical input in mine planning, ASEG Ext. Abstr. 2019 (1) (2019) 1–3.
[32] M. Brudy, H. Kjørholt, Stress orientation on the Norwegian continental shelf derived from borehole failures observed in high-resolution borehole imaging logs, Tectonophysics 337 (1–2) (2001) 65–84.
[33] P. Gaillot, T. Brewer, P. Pezard, et al., Borehole imaging tools- principles and applications, Sci. Drill. (5) (2007) 1–4.

Associate Prof. Jun Zhao's research is focused on rock rheology, safety monitoring, and disaster control for deep engineering. His academic contributions include the development of a series of true triaxial testing equipment for hard rocks, the development of a long-term intelligent integrated monitoring device for on-site rock masses and the elaboration of time-dependent fracturing mechanism of hard rocks in deep engineering. He is the secretary general of the National Technical Committee on Geotechnical Mechanics of Standardization Administration of China. He has received the Rocha medal from the International Society for Rock Mechanics and Rock Engineering (ISRM), the Future Leaders Program from the American Rock Mechanics Association (ARMA), and Innovation Talent Support Program from the China Postdoctoral Foundation.